RSC Advances




ROYAL SOCIETY OF CHEMISTRY

www.rsc.org/advances

**Full paper**

# Synthesis and characterization of bioreducible heparin-polyethyleneimine nanogels: application as imaging-guided photosensitizer delivery vehicle in photodynamic therapy

T. A. Debele[1], S. L. Mekuria[1], S.-Y. Lin[2], H. C. Tsai[1]*

## Abstract

Herein, we synthesized and characterized novel bioreducible heparin polyethyleneimine (HPC) nanogels consisted of heparin, branched polyethyleneimine (PEI) and L-cysteine. $^1$H-NMR and FTIR analysis confirmed the formation of HPC nanogels while TEM and dynamic light scattering revealed uniform spherical nanoparticles with average diameter of <200 nm. Zinc phthalocyanine (ZnPC) was encapsulated via the dialysis method and the drug is released in vitro from disulfide-containing HPC nanogels in a redox-sensitive manner at low pH. Additionally, HPC nanogels possess bright blue fluorescence which eliminates the use of additional probing agent in image-guided drug delivery. Moreover, singlet oxygen detection revealed that nanogels prevented ZnPc aggregation thus enhancing $^1O_2$ generation and photodynamic therapy (PDT) efficacy. These results showed that disulfide crosslinked HPC nanogels are promising vehicles for stimulated photosensitizer delivery in advanced PDT.

1. Graduate Institute of Applied Science and Technology, National Taiwan University of Science and Technology, Taipei 106, Taiwan, ROC.
2. National Applied Research Laboratories, Instrument Technology Research Center, Hsinchu 300, Taiwan, ROC.

[*] To whom correspondence and reprint requests should be addressed.

Prof. Hsieh-Chih Tsai

E-mail: h.c.tsai@mail.ntust.edu.tw

Tel: +886-2-27303625

Fax: +886-2-27303733

## Introduction

Photodynamic therapy (PDT) is a non-invasive combinatorial therapeutic modality for cancer that combines light, photosensitizer (PS), and oxygen. [1] When PSs in cells are exposed to specific wavelengths of light, they are transformed from the singlet ground state ($S_0$) to the excited singlet state, followed by intersystem crossing to the excited triplet state ($T_1$). The energy from $T_1$ is transferred to biological substrates and molecular oxygen generates reactive oxygen species ($^1O_2$, $H_2O_2$, $O_2^{\bullet}$, $^{\bullet}OH$) that cause cellular damage and tumor cell death through necrosis or apoptosis. [2] The majority of PSs currently on the market or under clinical trial is poorly water soluble, or hydrophobic, and thus have low bioavailability after intravenous administration. [3-6] Zinc phthalocyanine (ZnPc), a hydrophobic PS, is widely used for cancer PDT due to its high triplet yield, prolonged half-life, and preeminent singlet oxygen quantum yield. [7] Therefore, a technology platform that can effectively increase PS solubility and confer targeting potential is highly sought after. [8, 9] In recent years, numerous natural and synthetic macromolecular nanocarriers such as polymeric nanoparticles, liposomes, and micelles have been investigated and found to resolve challenges of intravenous administration and selective delivery to tumor sites. [10-12] Such targeted transportation of PSs into particular cells offers a novel alternative to conventional therapy in cancer management.

Hydrogels have received a great deal of attention due to their well-known three-dimensional physical structure, chemical tunability, high water content, and biocompatibility. [13] Natural biopolymers, for example, can be crosslinked to form biopolymer-based hydrogels through the high degree of available functional groups on most natural biopolymers. [14] Nanogels are dispersions of hydrogel nanoparticles formed from physically or chemically crosslinked polymeric networks that have been hailed as next generation drug delivery system due to their relatively high drug encapsulation capacity, diversity of drugs that can be encapsulated, uniformity, tunable size, ease of preparation, low toxicity, and responsiveness to external stimuli. [13, 15] Naturally-derived nanogels can be prepared from protein polymers, such as collagen, albumin, and fibrin, and polysaccharide polymers such as chitosan, hyaluronic acid, heparin, chondroitin sulfate, agarose, and alginate. [16, 17]

Heparin is a highly sulfated, biocompatible, biodegradable, water-soluble, and naturally-derived anionic polysaccharide composed of major repeating units of 2-O-sulfo-L-iduronic acid,

2-deoxy-2-sulfamino-6-O-sulfo-α-D-glucose, β-D-glucuronic acid, 2-acetamido-2-deoxy-α-D-glucose, and α-L-iduronic acid joined through 1→4 glycosidic linkages. [18] Functions of heparin include anticoagulation and inhibition of both angiogenesis and tumor growth. [19-22] Furthermore, present in heparin are numerous functional groups such as amino, hydroxyl, and carboxylic groups that provide opportunities of derivatization via chemical methods. [23] The most commonly used strategy is the derivation of the carboxyl and hydroxyl group which involves amidation and esterification respectively. [24-28] Several heparin-based micelles and gel nanoparticles have been chemically modified with cationic polymers such as branched polyethyleneimine and basic amino acids for use in field areas such drug carriers, gene delivery vehicles, and coating materials. [25, 29]

Polyethyleneimine (PEI) is a highly charged polyelectrolyte with protonated nitrogen on every third atom along the backbone. [30] Therefore, branched PEI has primary, secondary, and tertiary amine groups that can be protonated at different pH environments. [31, 32] Due to the protonable nitrogens in the polymer, PEI exhibits the "proton sponge" effect and absorbs protons in low pH environments such as the endosome which in turn chronologically increases proton influx, causes electrolyte imbalance, induces massive influx of chloride ions and water, and disrupts endosomes to release genes or drugs into the cytoplasm. [33-35] Furthermore, because PEI contains amine-rich nano-clusters and undergo electro-hole recombination, the polymer is fluorescent and can be used as imaging probe. [36] Currently, PEI (e.g. 25kDa, 1.8kDa) is utilized for various applications in drug delivery, gene delivery, and imaging. [37-39]

A stimuli-responsive nanogel drug delivery system (SRDDS) can realize zero premature release, respond to either external stimuli or local microenvironment differences, and release encapsulated drugs into the designated location. [40] External physical and chemical signals such as temperature, pH, and ions can alter carrier properties such as volume, molecular interactions, solubility, conformation, and crystallinity, all of which in turn affect the drug release mechanism. [1] In the case of pH-sensitive polymers, their swelling is controlled by various factors such as charge and pKa of the ionizable monomers, hydrophilicity, crosslinking density, ionic strength, and composition of the surrounding solution. [41] In biological systems, redox potential is another form of stimuli that results from the difference in the concentration of reduced glutathione in the intracellular matrix (2-10 mM) and extracellular matrix (2-20μM). Furthermore, results have

shown that the concentration of reduced glutathione is 4-fold higher in the cytosol of cancer cells in comparison to that of normal cells. [42, 43] Consequently, a variety of disulfide crosslinked nanocarriers and nanogels have been developed based on the introduction of cleavable disulfide linkages to the backbone, side chain, or crosslinker region of bioreducible systems. [44-46] Reductive-sensitive nanogels are stable in the extracellular environment and oxidized state but respond rapidly to intracellular glutathione (GSH) levels to release drugs into the cytosol and cell nucleus where most drugs take their therapeutic effect. [47]

In this study, we synthesized novel disulfide-crosslinked nanogels, prepared from heparin, branched PEI, and L-cysteine, to encapsulate photosensitizer ZnPc. Biocompatibility, encapsulation efficiency, imaging potential, pH- and redox-sensitive drug release property of the nanogels were studied. Their potential for PDT was evaluated using singlet oxygen sensor green (SOSG) to detect singlet oxygen generation after appropriate laser irradiation.

## Experimental

### Materials

Heparin sodium salt from porcine intestinal mucosa, zinc phthalocyanine (ZnPc), 2-(N-morpholino**)** ethanesulfonic acid hydrate (MES)**,** DL-dithiothreitol (DTT), branched polyethyleneimine (25kDa), and L-cysteine (L-Cys) were purchased from Sigma Aldrich. 1-ethyl-3-(3-dimethylaminopropyl) carbodiimide hydrochloride (EDC) and N-hydroxysuccinimide (NHS) were obtained from Acros Organics. Phosphate buffer saline (PBS) powder was purchased from Wako. Dulbecco's modified eagle medium (DMEM), penicillin, sodium pyruvate, trypsin, sterilized PBS, fetal bovine serum (FBS) and L-glutamine were purchased from Gibco. Dialysis bag (MWCO: 1, 6-8 and 12-14 kDa) was purchased from CelluSept T1. All other chemicals and reagents were of analytical grades and were purchased from commercial sources. Double distilled water was used in all processes.

### Preparation of HPC nanogels

Disulfide-crosslinked heparin polyethyleneimine (HPC) was prepared through amide bond formation that involved the amine groups of branched PEI, the amino group of L-Cys, and the carboxyl groups of heparin as depicted in **Scheme 1**. Briefly, 10 mg of heparin was dissolved in

MES buffer solution (5 mL, 0.01 M) and excess EDC and NHS (10 mg of EDC and 10 mg of NHS) were added to activate the carboxylic acid groups on heparin. After a 12 hr reaction at room temperature, different weight ratios of PEI and L-Cys, as shown in **Table 1**, were added under constant stirring. The reaction was carried out for 24 hr under room temperature. The HPC solution was then dialyzed (MWCO= 12-14 kDa) using distilled water for three days with water exchanged at 8 hr intervals. Lastly, HPC solution was passed through a syringe filter (pore size = 0.45μm) and lyophilized to obtain the final sponge-like HPC nanogel product which was stored for further use.

Characterization of HPC nanogels

Particle size and zeta-potential

Particle size and zeta potential of HPC nanogels were determined using a Nano ZS system (Zetasizer 3000HS, Malvern Instruments, UK). Briefly the samples were dispersed in deionized water, filtered (pore size 0.45μm), and sonicated for 10 min. A HeNe laser with 633 nm wavelength was used as the light source. Scattered light was detected at $90^{o}$ at $37^{o}$c. For each experiment, three sequences of 10 measurements each were performed.

Fourier transformed infrared spectroscopy (**FTIR**) analysis

Using a micropipette, 2-3 drops of a 1mg/ml of HPC nanogel solution (distilled water as the solvent) was transferred onto the center of a salts plate ($CaF_2$) and dried in a vacuum oven to obtain a homogeneous film. Samples were analyzed by a Perkin Elmer Spectrum FT-IR Spectrophotometer (Perkin Elmer, Waltham, MA, USA).

Nuclear magnetic resonance (**$^{1}$H-NMR**) analysis

2 mg of HPC was dissolved in $D_2O$ for sample preparation. The $^{1}$H NMR spectra for all starting materials and end product were recorded using a Varian Unity-600 (600 MHz) NMR spectrometer (Varian, Inc., Palo Alto, CA, USA). The trimethylsilane signal at δ=0.0ppm was used as a reference line.

Transmission electron microscopy (**TEM**)

1 mg of HPC was dissolved in distilled water and equilibrated at $37^{o}$C. A drop of the solution was placed on a carbon–copper grid (300-mesh, Ted Pella, Inc., USA) and air-dried for 24 hr.

The sample was then subjected to TEM observation using a FEI-TEM Philips TECNAI F20 system (Philips, Amsterdam, the Netherlands). [48]

Scanning electron microscopy (**SEM**)

The morphology of HPC nanogels was observed using field emission scanning electron microscopy (FESEM) (JSM-6500F, JEOL). Briefly 2 mg of HPC was dissolved in distilled water and a drop of the solution was placed on the SEM sample holder and air-dried for 2 days. The sample was then coated with platinum for 10 min prior to SEM observation.

Fluorescence spectrophotometer

The fluorescence intensity of HPC nanogels was assessed at 25 °C using a JASCO FP-8300 spectrophotometer (Jasco, Hachioji, Japan), equipped with Xenon lamp power supply and 1 cm-path quartz cell, at a slit width of 10 nm, scan rate of 240 nm/min, and PMT voltage 400 V. The excitation wavelength was fixed at 380 nm and the emission fluorescence was recorded in the 400-600 nm region.

In vitro cytotoxity

Cytotoxicity of HPC nanogels and PEI

The cytotoxicity of HPC nanogels and PEI was investigated. HeLa cells were grown in DMEM supplemented with 10% FBS, 1% penicillin, 1% glutamine, and 1% sodium pyruvate at 37$^{o}$C and 5% $CO_2$. Cells were seeded into 96-well plate at a density of $1 \times 10^5$ cells/well in complete DMEM medium and maintained in a humidified incubator at 37$^{o}$C in 5% $CO_2$ for 24 hr. Serial dilutions of HPC nanogels (0.1, 0.5, 1 and 2mg/mL) and PEI (0.1, 0.5, 1 and 2mg/mL) were added to the culturing medium in each well and incubated at 37$^{o}$C for 24 h. Cell viability of untreated cells was used as the control. The medium was removed and MTT solution was added and incubated at 37$^{o}$C for 4 hr. The resulting formazan crystals were solubilized using DMSO (100 μL) and absorbance was read using an enzyme-linked immunosorbent assay (ELISA) reader (Power Wave XS, BioTek, Winooski, VT) at 570 nm.

Results are expressed as the viable percentage of cells after treatments relative to untreated cells. Cell viability was calculated by following formula. [49]

$$\text{Cell viability \%} = \frac{\text{Absorbance of test cell} \times 100}{\text{Absorbance of controlled cell}}$$

Drug loading

Preparation of ZnPc-loaded nanogels

ZnPc-loaded HPC nanogels were prepared according to the direct dissolution method. [43] Briefly, 10 mg of HPC nanogel was dissolved in 5 mL of distilled water under constant stirring. Excess DTT (equivalent to cysteine used to prepare the nanogel) was mixed with the above solution in order to reduce disulfide bonds and maintain the sulfhydryl group of cysteine in reduced form (-SH). Then, 0.1 mg of ZnPc was dissolved in 5 mL of DMSO and mixed with the HPC nanogel solution. Disulfide bonds in HPC were formed by air oxidation and $H_2O_2$ for 12h. After drug loading, DMSO was removed through dialysis but unloaded ZnPc still remain in the dialysis bag. The mixture was then centrifuged at 5000 rpm for 30 minutes to remove unloaded ZnPc and the supernatant which contains ZnPc loaded HPC nanogels was lyophilized. The amount of ZnPc loaded was determined by a colorimetric method. Briefly, 1 mg of the lyophilized ZnPc-loaded HPC nanogel was dissolved in 4 mL of DMSO in the presence of DTT and sonicated for 15 minutes to extract ZnPc until a clear solution remained in the bath sonicator. Absorbance of the solution extract was measured using a UV-Vis spectrophotometer. A standard curve was constructed from ZnPc prepared at various concentrations in DMSO (0.1, 0.05, 0.01, 0.005, 0.001, 0.0005 and 0.0001mM).

The drug entrapment efficiency (EE) was calculated by using the following equations:-

$$EE = \frac{\text{Amount of ZnPc in nanoparticles} \times 100}{\text{Initial amount of ZnPc-used for loading}}$$

Detection of singlet oxygen generation

Singlet oxygen ($^1O_2$) generated from photosensitizer ZnPc was measured by singlet oxygen sensor green (SOSG). [50] The SOSG solution was prepared by dissolving 100 µg of SOSG in 33 µL of methanol in dim condition immediately prior to use. To each solution containing ZnPc (1 µM, 5mL $D_2O$) or ZnPc-loaded HPC nanogel (1 µM, 5mL $D_2O$), 1µL of SOSG (1 µM) was added. Measurements were made for 120 minutes with 10-minute intervals between each measurement. Laser irradiation at 808 nm was used to photosensitize ZnPc and generate $^1O_2$. Fluorescence emission spectrum between 450 and 750 nm was recorded for SOSG before and after reaction with $^1O_2$. The increase in fluorescence intensity of SOSG (excitation/emission of

482/535-540 nm) as a result of singlet oxygen generation was monitored using a spectrofluoro photometer. [51]

Drug release study

ZnPc release from HPC nanogels

The in vitro release of ZnPc from nanogels was assessed in 0.01mM MES buffers at pH of 5.5 and 7.4 using the dialysis method. [18] Briefly, 3 mL of the ZnPc solution (1mg/5mL DMSO) was mixed with the HPC solution (2mg/mL) and dialyzed against distilled water for 24 hr to remove DMSO. Drug release was measured by dialyzing 2mL of the ZnPc-HPC solution in 6-8 kDa MWCO membrane against 10 mL of the corresponding release medium containing 2% v/v of Triton x-100 at 25$^{o}$C to ensure sink conditions and under constant stirring to prevent ZnPc aggregation. At each predetermined time point, absorbance of the releasing medium was measured and the medium was completely exchanged with equal amount of fresh releasing medium. Four release media including 0.01 M MES (pH 5.5 and 7.4) and 0.01 M MES containing 2mg/mL GSH (pH 5.5 and 7.4) were used to study pH and GSH dependent drug release. The ZnPc concentration was determined using a pre-established calibration curve. Results are expressed as cumulative release % over time ± standard deviation of three experiments. [49]

Cellular uptake study of ZnPc-loaded HPC nanogels by confocal microscopy

HeLa cells were grown in DMEM supplemented with 10% FBS, 1% penicillin, 1% glutamine, and 1% sodium pyruvate at 37$^{o}$C and 5% $CO_2$. Cells were seeded in 35 mm glass bottom culture dish at a density of 2.5 $\times 10^5$ cells per well and incubated at 37$^{o}$C with 5% $CO_2$ for 24 hr. Thereafter, cells were co-incubated with ZnPc-loaded HPC nanogel (0.01mM), ZnPc (0.01mM), and HPC nanogel (0.5mg/ml) for 24 h at 37$^{o}$C. The cells were washed three times with PBS prior to visualization using a Leica TCS-SP2 confocal laser scanning microscope (CLSM) (Leica, Wetzlar, Germany) at the excitation wavelength of 420 nm and 600 nm and emission wavelength of 450-600 nm and 620–800 nm for HPC nanogel and ZnPc respectively. Results were acquired and analyzed using Leica LASAF Lite software. [49]

Photodynamic cytotoxicity of ZnPc-HPC nanogels and ZnPc

The MTT method was used to study the photodynamic cytotoxic effect. [52] HeLa cells were seeded into a 96-well plate at a density of $1 \times 10^5$ cells/well in complete DMEM medium and grown for 24 hr at 37°C. Then, ZnPc-loaded HPC (0.01, 0.02, 0.05, 0.1mg/mL, based on concentration of ZnPc) and ZnPc (0.01, 0.02, 0.05, 0.1mg/mL) were added to each well. After 24 hr incubation, the medium in each well was removed and cells were washed three times with PBS. Fresh complete DMEM medium (100 μL) was added into each well and after 4 hr incubation, the cells were exposed to 532 nm laser light for an hour followed by further incubation for 24 hr. MTT assay was conducted by replacing the medium in each well with a new medium containing MTT (20 μL, 5 mg/mL). The medium was removed after 4 hr and 100μL DMSO was added to each well to solubilize the formazan crystals. The plate was gently shaken for 15 minutes and its absorbance read at 565 nm using a TECAN Safire microplate reader (Tecan, Maennedorf, Switzerland). ZnPc-HPC and ZnPC without light irradiation were used as control groups. Results are expressed as the viable percentage of cells after various treatments relative to the control cells without any treatment. Cell viability was calculated by following formula. [49]

$$\text{Cell viability \%} = \frac{\text{Absorbance of test cell} \times 100}{\text{Absorbance of controlled cell}}$$

**Results and discussion**

Preparation and characterization of HPC nanogels

Heparin is one of the most abundant sulfated glycosaminoglycan (GAGs) that possess anti-cancer activities and is often used as a nanocarrier in micelle or nanogel form to transport different photosensitizers for PDT. [51, 53] Modification of the carboxyl groups of heparin has been studied by several groups and typically involved amidation using amino containing compounds such as aminated deoxycholic acid, fluorescent amines, aminated retinoic acid, aminated folic acid, and amino acids in the presence of EDC/NHS coupling agents. [24-28] The goal of this study was to prepare a bioreducible heparin derivative from heparin, PEI, and L-Cys by amide bond formation between functional groups. First, the carboxyl groups on heparin were activated using excess EDC/NHS and then reacted with the amino group of L-Cys and amine groups of branched PEI as shown in **Scheme 1**. The L-Cys carboxyl group and PEI amino groups can also react to

form stable bonds. Most crucially, L-Cys has the tendency to form disulfide linkages through its side chain SH group to confer reduction-sensitivity.

The chemical compositions of HPC conjugates were confirmed by FTIR (**Figure 1**) and $^{1}$H NMR spectroscopy (**Figure 2**). The chemical compositions of HPC conjugates were confirmed by FTIR (**Figure 1**) and $^{1}$H NMR spectroscopy (**Figure 2**). Based on the results shown in Figure 1, heparin exhibited the -OH stretching at 3454 $cm^{-1}$ and the C=O stretching at 1615 $cm^{-1}$. The spectrum of HPC possessed additional absorption bands compared to heparin, which is located at 1561$cm^{-1}$ (N-H bending) which confirms amide bond formation between carboxyl group of heparin and amine group of PEI and L-Cys. Moreover HPC nanogels possess peaks at 2852-2956 cm-1 which can be attributed to C-H stretch of PEI and peak at 3350 $cm^{-1}$, which is from the broad –OH stretch of heparin. Furthermore, unlike IR spectrum of L-Cys which has peak at 2550 $cm^{-1}$, HPC nanogels does not shows any peaks at 2550 $cm^{-1}$which confirms that SH group of L-Cys in HPC nanogels forms disulfide linkage.

In addition, the $^{1}$H-NMR spectrum of HPC nanogels also confirms conjugation of PEI and L-Cys on the heparin. $^{1}$H-NMR of the major repeating monosaccharide of heparin, glucose amine, glucouronic acid and Iduronic acid where find from 3.26-5.6 ppm and the spectrum region at 1.8-2.2ppm indicates the proton signal of acetyl groups of heparin. [54] Similarly, $^{1}$H-NMR of PEI where found at 2.4-3.05 ppm in HPC nanogels which also indicates successful conjugation between heparin and PEI. Furthermore, proton signal of L-Cys is also found around 3.05-3.2 and 4.02-4.03ppm which partially overlaps with proton signal of PEI and heparin respectively. The majority of proton signal intensity from heparin (3.26-5.6 ppm) was shielded to (3.3-4.3 ppm) in the nanogel and this is may be due to the heparin was covered with highly branched PEI. The decrease of proton signal of core materials also reported in previous study. [55, 56]

The particle size, zeta potential, and polydispersity index (PDI) of the nanogels prepared at different feeding ratios (w/w) are presented in **Table 1**. The weight ratio of PEI and L-Cys was varied at a fixed heparin weight. Zeta potential measurement provides important information on nanogel formation due to the difference in charge between cationic PEI and anionic heparin. All nanogels synthesized were positively charged which indicates the neutralization of heparin with PEI. As expected, increasing the PEI ratio resulted in greater zeta potential due to the presence of multiple amino groups on branched PEI. The magnitude of zeta potential, or surface charge, on the other hand, gives valuable prediction of the electrostatic repulsion between charged particles

which is crucial to maintaining colloid stability. For HPC nanogels, there was an inverse relationship between zeta potential and size. Nanogels with smaller particle size were more densely charged because greater charge likely prevented particle aggregation and growth in overall particle size. HPC nanogels were well dispersed with mean average particle size of 165.7 ± 5.8, 134.6 ± 49.9 and 117.4 ± 20.6 nm and zeta potential of 35.47 ± 1.04, 43.4 ± 1.32 and 48.5 ± 0.4mV for $HPC_{0.75,}$ $HPC_1$ and $HPC_3$ respectively. Moreover, TEM microscopy (**Figure 4a**) revealed monodispersed HPC nanogels with mean particle size of 100-120 nm. The slight discrepancy between the size obtained from TEM and dynamic light scattering is due to the former being a representation of dry particle size while the latter provides estimation of the hydrodynamic diameter in water. Since HPC nanogels likely absorb large amounts of water, dry HPC nanoparticles 100-120 nm in size can swell to nanogels with a mean average size of 165.7 ± 5.8nm.

Although PEI is widely used alone or in combination with other polymers, the toxicity of PEI persists as a problem due to its cationic nature. In order to investigate cytotoxicity, cell viability was determined after cells were treated with different concentrations of the nanogel and PEI, as summarized in **Figure 3**. Results show that >75% viability was maintained at low concentrations of HPC nanogel (0.1 and 0.5 mg/mL) while further increase in concentration resulted in significant increase in cytotoxicity. However, at all concentrations, branched 25 kDa PEI exhibited significant toxicity toward cells and resulted in <10% viability. The direct relationship between PEI content and cell toxicity confirms that cationic amino groups of PEI are the main cause of cell toxicity. According to these results, low concentration HPC nanogel (<0.5 mg/mL) with low PEI weight ratio can be used as a carrier for photosensitizers. By taking this into consideration, $HPC_{0.75}$ was selected for drug delivery and other experiments in the latter part of this work.

The morphology of HPC nanogels was visualized by TEM and SEM and revealed to be spherical and uniformly distributed as shown in **Figure 4a** and **Figure 4b** respectively. Furthermore, elemental analysis of HPC nanogels was conducted using energy dispersive X-ray spectroscopy (EDS) and the presence of carbon, nitrogen, oxygen, and sulfur supports the inclusion of all three major components.

Fluorescence properties of HPC nanogels

Fluorescence spectroscopy revealed that when HPC nanogel solutions were excited at a wavelength of 380 nm, fluorescence intensity was increased in comparison to the weakly fluorescent PEI at the emission wavelength of 400-600 nm (**Figure 5**). The fluorescence emission intensity increment of PEI in the presence of heparin may be due to the covalent conjugation followed cross linking and electrostatic interactions between the amino (protonated amino) group in PEI and sulfate and carboxylate groups in heparin. [57, 58] Furthermore, as the weight ratio of PEI increases, relatively fluorescence emission intensity of the HPC nanogels also increased ($HPC_3 > HPC_1 > HPC_{0.75}$), which is may be due to aggregation induced emission enhancement. [59] Similarly various researchers reported that, the linear relationships between dendrimers concentration and fluorescence emission intensity (i.e. fluorescence intensity increase as the concentration of dendrimers increase) which almost has similar structure with branched PEI. [60, 61] Hence, cellular uptake and distribution of HPC nanogels can be visualized directly without probing agents and red-shift of fluorescence which are appropriate for in vitro and in vivo imaging.

ZnPc loading in HPC nanogels

Loading of ZnPc into HPC nanogel is depicted in **Scheme 2**. Before drug loading, the DTT was used to reduce the disulfide linkage to facilitate more entrapment of ZnPc in the HPC nanogels. Then the $H_2O_2$ was added to re-introduce disulfide linkage (S-S)) which further increases the hydrophobic nature of HPC nanogels matrix. Since the ZnPc is a hydrophobic photosensitizer, it was loaded in hydrophobic region of HPC nanogels matrix in physical encapsulation. A ZnPc solution at the concentration of 0.1 mg/mL was used in order to ensure the monomeric state of ZnPc in ZnPc-loaded HPC nanogels. ZnPc in DMSO has a characteristic absorption maximum at 672 nm. The loaded ZnPc was extracted by sonicating lyophilized ZnPc-loaded HPC nanogels (1mg/4ml using DMSO) and was quantified by UV-Vis as shown in **Figure 6a**. The encapsulation efficiency was calculated approximately 40.3 ± 1.6 %. The particle size of HPC nanogels are significantly decreased when hydrophobic ZnPc loaded to it. This is may be due to strong hydrophobic interaction between hydrophobic ZnPc and hydrophobic region of HPC nanogels matrix, which further drove more water out of a particles and decreasing the particle size of nanogels. Zeta potential of HPC nanogel is slightly increased when

encapsulated with ZnPc from 35.47 ± 1.04 mV to 46.33 ± 1.05 mV. Moreover, fluorescence emission measurement of the ZnPc loaded in HPC nanogel shows a red shift (**Figure 6b**). Fluorescence band shifts for red in the used media (DMSO) may be related with the incorporation of the ZnPc into hydrophobic matrix of nanogels. [62] Furthermore the red shift band may be due to J-aggregation of the ZnPc in the HPC Nanogel.

In vitro drug release

Redox potential is a unique intracellular signal that can be exploited to activate drug release inside tumor cells and tumor tissues. As shown in **Figure 7**, only 2% of the ZnPc was released after 30 minutes in the absence of GSH at both pH values while 12% of the photosensitizer was released at pH 5.5 in the presence of reduced glutathione. Approximately 43% and 30.8% of ZnPc was released after 48 hr at pH 5.5 in the presence and absence of GSH respectively. While relatively lower drug release was observed in the presence and absence of GSH at pH 7.4 which seems statistically insignificant. Although the cleavage of disulfide bonds takes place in a reducing environment, HPC nanogel was still stable due to the existence of chemical linkage between heparin and PEI at pH 7.4. On the contrary, the PEI of HPC nanogels can be protonated at low pH value (pH 5.5) and nanogels undergo swelling, which further enhance ZnPc release in the presence of GSH. These results agree with the prediction that reduced GSH functions as a reducing agent in disulfide cleavage to facilitate ZnPc release from the HPC nanogel matrix at pH 5.5. Hence, in comparison to the pH 7.4, the effects of GSH is much clearly seen at pH 5.5, this shows redox sensitive drug release from HPC nanogels has synergistic effects with proton sponge effects of PEI. In summary, the low pH and high GSH concentration in cancer cells both act to govern the rate of ZnPc release from HPC nanogel.

Detection of singlet oxygen generation

When PSs are exposed to specific wavelengths of light they are transformed from the ground state ($PS_0$) to an excited singlet state ($^1PS$) followed by intersystem crossing to an excited triplet state ($^3PS$) which transfers energy to molecular oxygen and generates reactive oxygen species (ROS). [1] The singlet oxygen ($^1O_2$) is one of the well-known ROS responsible for the destruction of target cancer cells in PDT. [63] Therefore, the ability of PSs to generate $^1O_2$ upon irradiation with a light source is the most important index in PDT. As a reagent, SOSG is highly selective for $^1O_2$ and does not show noticeable response to superoxide or hydroxyl radicals. [64] **Figure 8a**

shows that the fluorescent intensity of SOSG was noticeably higher after reacting with irradiated PSs. The maximum emission peak of SOSG endoperoxide (SOSG-EP) at 530-540 nm is the result of SOSG reacting with $^1O_2$. A major concern of ZnPc which limits its application in the physiological environment is its tendency to severely aggregate and lose $^1O_2$ generation efficiency. As shown in **Figure 8b**, HPC nanogels prevented the aggregation of ZnPc and maintained ZnPc in monomeric form, thus generating more $^1O_2$ to react with SOSG and increase the fluorescence intensity. On the other hand, histidine (His) served as a quencher by scavenging $^1O_2$ and decreasing its availability. The increase in SOSG fluorescent intensity as a function of time due to singlet oxygen generation from ZnPc, as shown in **Figure 8c**, suggests that the HPC nanogel is a well-suited candidate vesicle for ZnPc to enhance PDT activity.

Cellular uptake of ZnPc-loaded HPC nanogels

Cellular uptake of ZnPc-loaded HPC nanogel by HeLa cells after 24 hr co-incubation was examined by CLSM. **Figure 9a** shows the typical morphology of HeLa cells under bright field microscopy. The bright blue color in **Figure 9b** is attributed to the fluorescence of HPC nanogels while the scattered red fluorescence in the cytoplasm as shown in **Figure 9c** comes from the ZnPc PSs. A merged image (**Figure 9d**) reveals that ZnPc-loaded HPC nanogels were internalized by the cells, likely through endocytosis, and the ZnPc was released from the nanogels in the presence of reduced GSH. Hence, HPC nanogels can be used simultaneously as drug carrier and imaging probe due to its fluorescence property.

Photodynamic cytotoxicity effect of ZnPc-HPC nanogels and ZnPc

Photodynamic cytotoxicity of free ZnPc and ZnPc-loaded HPC nanogels were evaluated before and after irradiation using a 532 nm laser light source. As shown in **Figure 10a** and **10b**, PDT using ZnPc-HPC nanogels and free ZnPc resulted in significant cell death at concentrations of 0.01 mg/mL to 0.1 mg/mL. In addition, the photoactivated cytotoxicity of ZnPc and ZnPc-HPC was dose dependent due to correlation with the amount of singlet oxygen generated in the presence of an appropriate light source. Even at a low concentration of 0.01 mg/mL, photoactivated free ZnPc eradicated approximately 85% of HeLa cells. On the other hand, ZnPc-loaded nanogels resulted in even greater cytotoxicity due to better dispersion of the photosensitizer. In the absence of laser irradiation, cytotoxicity that is independent of singlet oxygen generation was observed. These results, in combination, show that ZnPc is an effective

PDT agent and that the described nanogel carrier system further increased the efficacy of the treatment.

## Conclusion

The multifunctional nanogel system that is redox-sensitive (at low pH) and fluorescent in nature, as described in this study, not only eliminates the need of an additional imaging probe but also ensures that the photosensitizers are released into the cytoplasm where they are permitted to take their full effect once they are internalized into cells. The positively charged nanogels were approximately 100-170 nm in size and crosslinked with bioreducible disulfide bonds which were cleaved once the nanogels were internalized into cells. Confocal microscopy revealed that HPC nanogels were transported across the cellular membrane and their innate blue fluorescence makes possible image-guided delivery without the use of probing agents. The described nanogel also enhanced $^1O_2$ generation by preventing ZnPc aggregation. Taken together, HPC nanogels provide multiple advantages and thus is a promising new vesicle for photosensitizer delivery to enhance PDT efficacy.

## Acknowledgements

The authors would like to thank the Ministry of Science and Technology, Taiwan (MOST 103-2221-E-011-035) and the National Taiwan University of Science and Technology (102H451201) for providing financial support.

## Reference

1. T. Debele, S. Peng and H.-C. Tsai, *International journal of molecular sciences*, 2015, **16**, 22094.
2. R. R. Allison and K. Moghissi, *Clinical endoscopy*, 2013, **46**, 24-29.
3. A. E. O'Connor, W. M. Gallagher and A. T. Byrne, *Photochemistry and photobiology*, 2009, **85**, 1053-1074.
4. A. Ormond and H. Freeman, *Materials*, 2013, **6**, 817-840.

5. J. J. Schuitmaker, P. Baas, H. L. van Leengoed, F. W. van der Meulen, W. M. Star and N. van Zandwijk, *Journal of photochemistry and photobiology. B, Biology*, 1996, **34**, 3-12.
6. S. S. Stylli, A. H. Kaye, L. MacGregor, M. Howes and P. Rajendra, *Journal of clinical neuroscience : official journal of the Neurosurgical Society of Australasia*, 2005, **12**, 389-398.
7. P. Khoza, E. Antunes and T. Nyokong, *Polyhedron*, 2013, **61**, 119-125.
8. B. Felice, M. P. Prabhakaran, A. P. Rodriguez and S. Ramakrishna, *Materials science & engineering. C, Materials for biological applications*, 2014, **41**, 178-195.
9. H. P. Lassalle, M. Wagner, L. Bezdetnaya, F. Guillemin and H. Schneckenburger, *Journal of photochemistry and photobiology. B, Biology*, 2008, **92**, 47-53.
10. M. Sadasivam, P. Avci, G. K. Gupta, S. Lakshmanan, R. Chandran, Y.-Y. Huang, R. Kumar and M. R. Hamblin, *European journal of nanomedicine*, 2013, **5**, 10.1515/ejnm-2013-0010.
11. L. Li and K. M. Huh, *Biomaterials Research*, 2014, **18**, 19.
12. L. Gibot, A. Lemelle, U. Till, B. Moukarzel, A. F. Mingotaud, V. Pimienta, P. Saint-Aguet, M. P. Rols, M. Gaucher, F. Violleau, C. Chassenieux and P. Vicendo, *Biomacromolecules*, 2014, **15**, 1443-1455.
13. J. K. Oh, R. Drumright, D. J. Siegwart and K. Matyjaszewski, *Progress in Polymer Science*, 2008, **33**, 448-477.
14. Y. C. Ho, F. L. Mi, H. W. Sung and P. L. Kuo, *Int J Pharm*, 2009, **376**, 69-75.
15. R. T. Chacko, J. Ventura, J. Zhuang and S. Thayumanavan, *Advanced drug delivery reviews*, 2012, **64**, 836-851.
16. T. R. Hoare and D. S. Kohane, *Polymer*, 2008, **49**, 1993-2007.
17. E. M. Ahmed, *Journal of Advanced Research*, 2015, **6**, 105-121.
18. L. Li, H. T. Moon, J.-Y. Park, Y. J. Heo, Y. Choi, T. H. Tran, Y.-k. Lee, S. Y. Kim and K. M. Huh, *Macromolecular Research*, 2011, **19**, 487-494.
19. L. Huang and R. J. Kerns, *Bioorganic & medicinal chemistry*, 2006, **14**, 2300-2313.
20. S. A. Mousa and L. J. Petersen, *Thrombosis and haemostasis*, 2009, **102**, 258-267.
21. K. Norrby, *Pathophysiology of Haemostasis and Thrombosis*, 1993, **23**, 141-149.
22. J. P. Ritchie, V. C. Ramani, Y. Ren, A. Naggi, G. Torri, B. Casu, S. Penco, C. Pisano, P. Carminati, M. Tortoreto, F. Zunino, I. Vlodavsky, R. D. Sanderson and Y. Yang, *Clinical*

*cancer research : an official journal of the American Association for Cancer Research*, 2011, **17**, 1382-1393.

23. Z. Xu, G. Shen, X. Xia, X. Zhao, P. Zhang, H. Wu, Q. Guo, Z. Qian, Y. Wei and S. Liang, *Journal of translational medicine*, 2011, **9**, 46-46.
24. X. Yang, H. Du, J. Liu and G. Zhai, *Biomacromolecules*, 2015, **16**, 423-436.
25. K. S. Jee, H. D. Park, K. D. Park, Y. H. Kim and J.-W. Shin, *Biomacromolecules*, 2004, **5**, 1877-1881.
26. W. Guo and R. J. Lee, *AAPS PharmSci*, 1999, **1**, 20-26.
27. S. I. Weiss, N. Sieverling, M. Niclasen, C. Maucksch, A. F. Thunemann, H. Mohwald, D. Reinhardt, J. Rosenecker and C. Rudolph, *Biomaterials*, 2006, **27**, 2302-2312.
28. G. Jiang, K. Park, J. Kim, K. S. Kim, E. J. Oh, H. Kang, S. E. Han, Y. K. Oh, T. G. Park and S. Kwang Hahn, *Biopolymers*, 2008, **89**, 635-642.
29. K. Park, K. Kim, I. C. Kwon, S. K. Kim, S. Lee, D. Y. Lee and Y. Byun, *Langmuir*, 2004, **20**, 11726-11731.
30. J. Ziebarth and Y. Wang, *Biophysical Journal*, 2009, **97**, 1971-1983.
31. C. K. Choudhury and S. Roy, *Soft Matter*, 2013, **9**, 2269-2281.
32. C. Sun, T. Tang, H. Uludağ and Javier E. Cuervo, *Biophysical Journal*, 2011, **100**, 2754-2763.
33. O. Boussif, F. Lezoualc'h, M. A. Zanta, M. D. Mergny, D. Scherman, B. Demeneix and J. P. Behr, *Proc. Natl. Acad. Sci. U. S. A.*, 1995, **92**, 7297-7301.
34. M. Jager, S. Schubert, S. Ochrimenko, D. Fischer and U. S. Schubert, *Chemical Society reviews*, 2012, **41**, 4755-4767.
35. A. K. Varkouhi, M. Scholte, G. Storm and H. J. Haisma, *Journal of controlled release : official journal of the Controlled Release Society*, 2011, **151**, 220-228.
36. L. Pastor-Pérez, Y. Chen, Z. Shen, A. Lahoz and S. E. Stiriba, *Macromolecular rapid communications*, 2007, **28**, 1404-1409.
37. J. Zhang, D. Fang, Q. Ma, Z. He, K. Ren, R. Zhou, S. Zeng, B. Li, L. He, G. He and X. Song, *Macromolecular Chemistry and Physics*, 2014, **215**, 163-170.
38. I. C. Bellettini, L. G. Nandi, R. Eising, J. B. Domingos, V. G. Machado and E. Minatti, *Journal of Colloid and Interface Science*, 2012, **370**, 94-101.

39. Y. Sun, W. Cao, S. Li, S. Jin, K. Hu, L. Hu, Y. Huang, X. Gao, Y. Wu and X.-J. Liang, *Scientific reports*, 2013, **3**.
40. F. Tang, L. Li and D. Chen, *Advanced Materials*, 2012, **24**, 1504-1534.
41. S. Mura, J. Nicolas and P. Couvreur, *Nat Mater*, 2013, **12**, 991-1003.
42. J. M. Estrela, A. Ortega and E. Obrador, *Critical reviews in clinical laboratory sciences*, 2006, **43**, 143-181.
43. N. Dai Hai, C. Jong Hoon, J. Yoon Ki and P. Ki Dong, *Journal of Bioactive and Compatible Polymers*, 2011, **26**, 287-300.
44. Z. Q. Yu, J. T. Sun, C. Y. Pan and C. Y. Hong, *Chemical communications*, 2012, **48**, 5623-5625.
45. P. Li, Z. Luo, P. Liu, N. Gao, Y. Zhang, H. Pan, L. Liu, C. Wang, L. Cai and Y. Ma, *Journal of controlled release : official journal of the Controlled Release Society*, 2013, **168**, 271-279.
46. Z.-K. Wang, L.-H. Wang, J.-T. Sun, L.-F. Han and C.-Y. Hong, *Polymer Chemistry*, 2013, **4**, 1694-1699.
47. M. M. Kemp and R. J. Linhardt, *Wiley Interdisciplinary Reviews: Nanomedicine and Nanobiotechnology*, 2010, **2**, 77-87.
48. A. A. Sobczuk, S.-i. Tamaru and S. Shinkai, *Chemical communications*, 2011, **47**, 3093-3095.
49. W. Wu, W. Yao, X. Wang, C. Xie, J. Zhang and X. Jiang, *Biomaterials*, 2015, **39**, 260-268.
50. A. Gollmer, J. Arnbjerg, F. H. Blaikie, B. W. Pedersen, T. Breitenbach, K. Daasbjerg, M. Glasius and P. R. Ogilby, *Photochemistry and photobiology*, 2011, **87**, 671-679.
51. L. Li, B.-c. Bae, T. H. Tran, K. H. Yoon, K. Na and K. M. Huh, *Carbohydrate polymers*, 2011, **86**, 708-715.
52. X. Ma, S. Sreejith and Y. Zhao, *ACS applied materials & interfaces*, 2013, **5**, 12860-12868.
53. E. Jorpes, *Biochemical Journal*, 1935, **29**, 1817-1830.
54. H. Liu, Z. Zhang and R. J. Linhardt, *Natural product reports*, 2009, **26**, 313-321.
55. M.-C. Jones, M. Ranger and J.-C. Leroux, *Bioconjugate Chemistry*, 2003, **14**, 774-781.

56. L. Luo, M. Ranger, D. G. Lessard, D. Le Garrec, S. Gori, J.-C. Leroux, S. Rimmer and D. Smith, *Macromolecules*, 2004, **37**, 4008-4013.
57. Y. Sun, W. Cao, S. Li, S. Jin, K. Hu, L. Hu, Y. Huang, X. Gao, Y. Wu and X.-J. Liang, *Scientific Reports*, 2013, **3**, 3036.
58. M. Wang, D. Zhang, G. Zhang and D. Zhu, *Chemical communications*, 2008, DOI: 10.1039/B808877B, 4469-4471.
59. J. Liu, Y. Zhong, J. W. Y. Lam, P. Lu, Y. Hong, Y. Yu, Y. Yue, M. Faisal, H. H. Y. Sung, I. D. Williams, K. S. Wong and B. Z. Tang, *Macromolecules*, 2010, **43**, 4921-4936.
60. Y. Wang, S. Niu, Z. Zhang, Y. Xie, C. Yuan, H. Wang and D. Fu, *Journal of nanoscience and nanotechnology*, 2010, **10**, 4227-4233.
61. D. Wang and T. Imae, *Journal of the American Chemical Society*, 2004, **126**, 13204-13205.
62. M. N. Sibata, A. C. Tedesco and J. M. Marchetti, *Eur J Pharm Sci*, 2004, **23**, 131-138.
63. B. V. Chernyak, D. S. Izyumov, K. G. Lyamzaev, A. A. Pashkovskaya, O. Y. Pletjushkina, Y. N. Antonenko, D. V. Sakharov, K. W. A. Wirtz and V. P. Skulachev, *Biochimica et Biophysica Acta (BBA) - Bioenergetics*, 2006, **1757**, 525-534.
64. H. Lin, Y. Shen, D. Chen, L. Lin, B. C. Wilson, B. Li and S. Xie, *Journal of fluorescence*, 2013, **23**, 41-47.

## Scheme, figure and Table

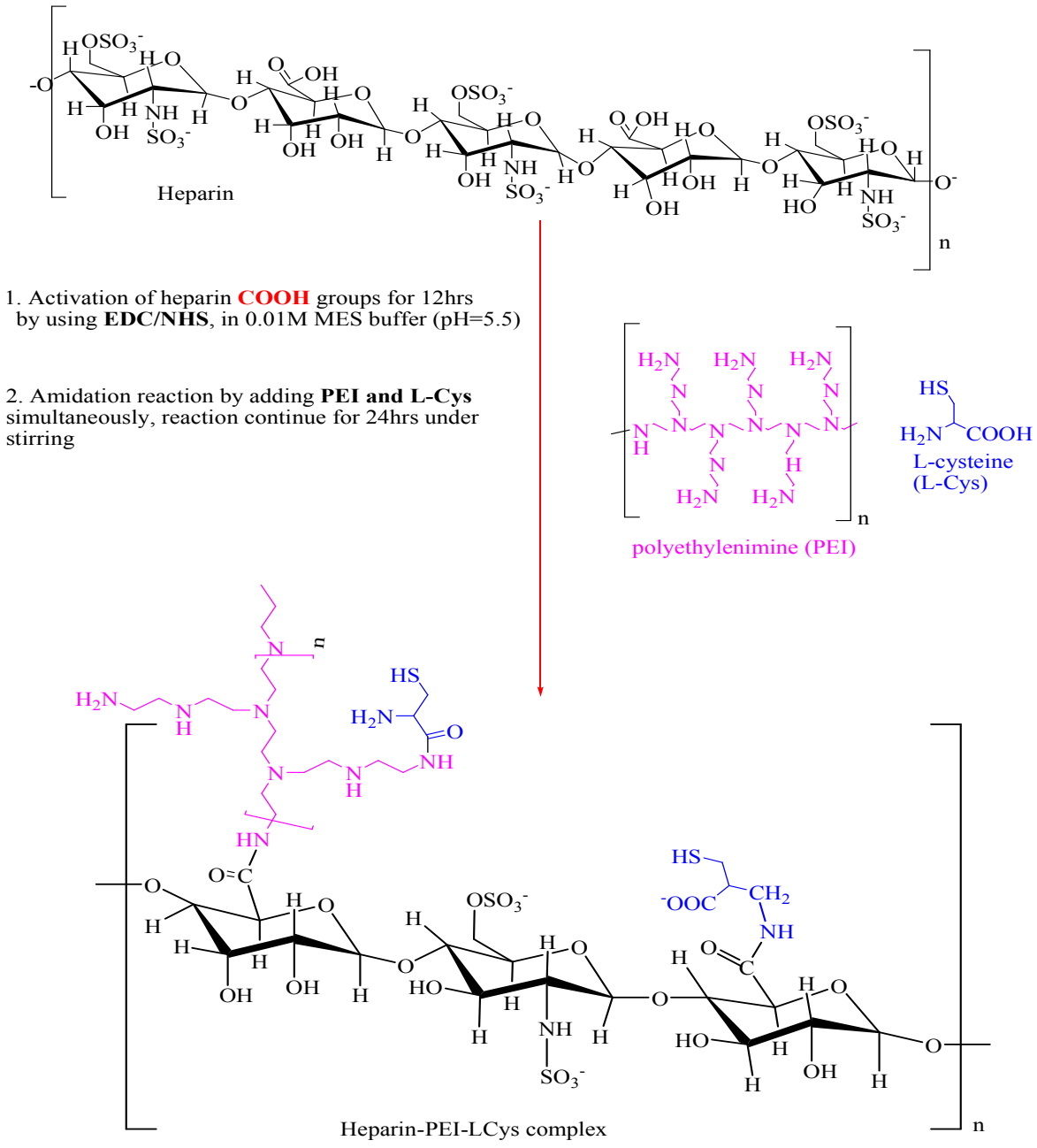


**Scheme 1.** Activation and amidation of heparin for the synthesis of heparin-PEI-L-Cys (HPC) complex

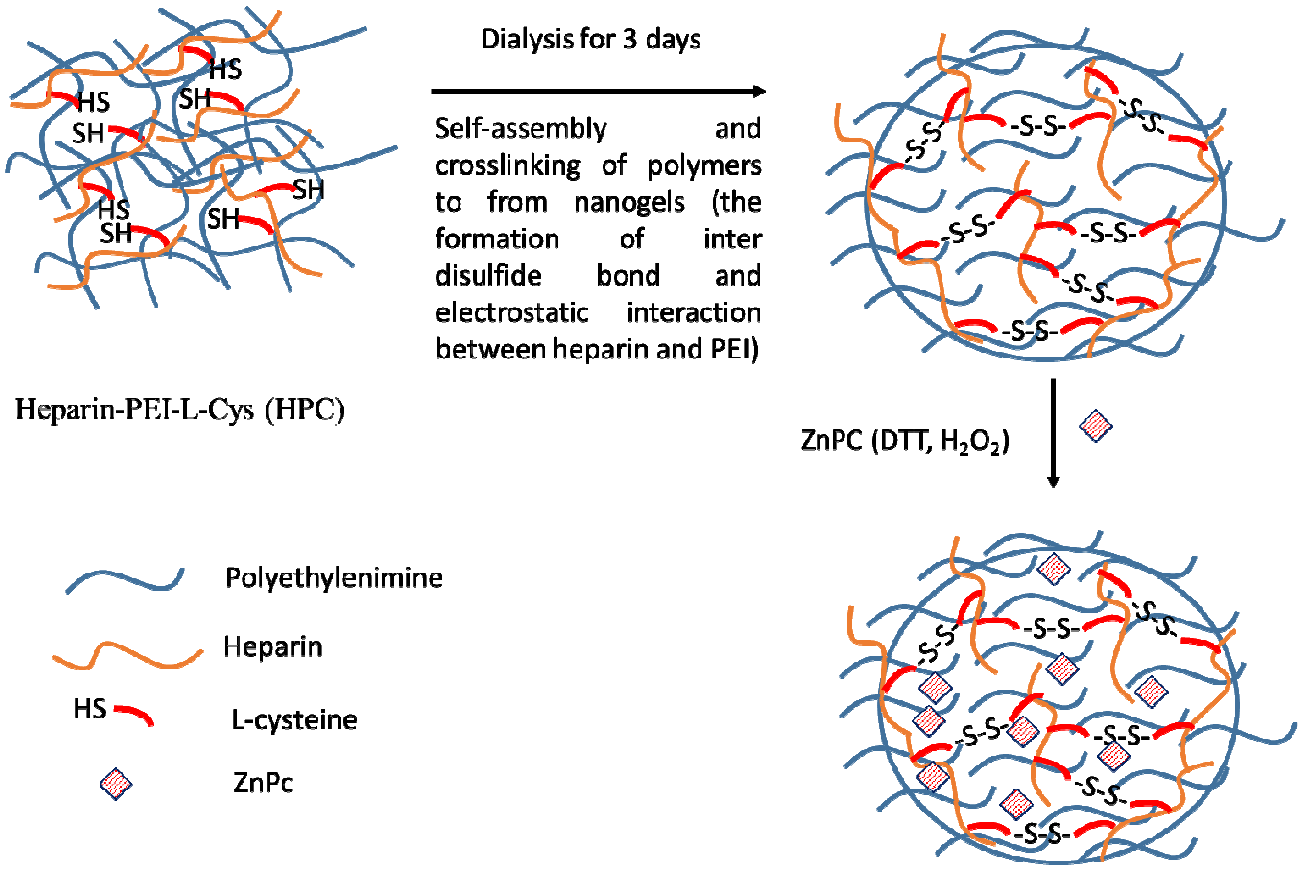


**Scheme 2**. Schematic diagram of HPC nanogel preparation and ZnPc loading

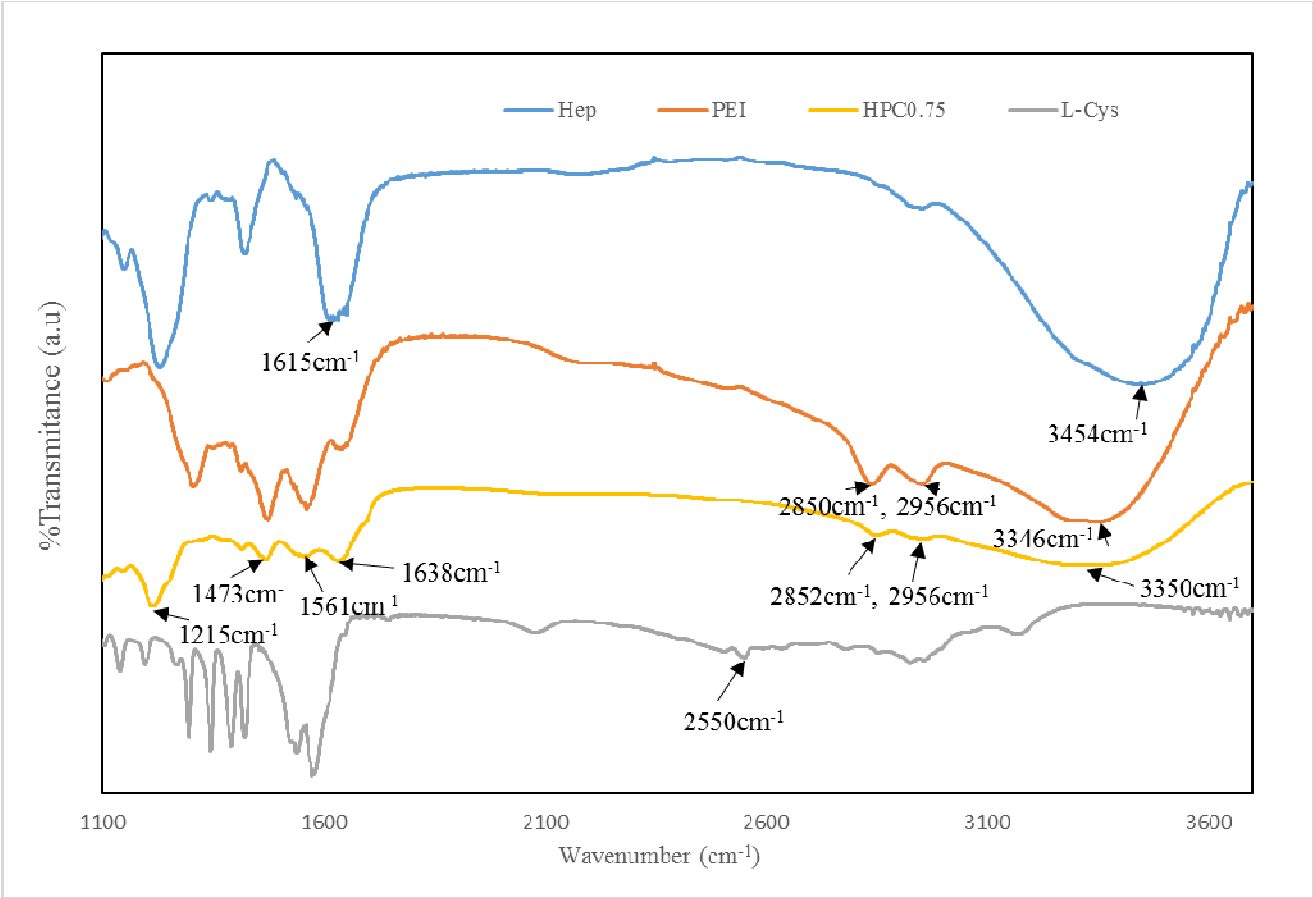


**Figure 1**. The FT-IR spectra of heparin, PEI, L-Cys, and their complex $HPC_{0.75}$

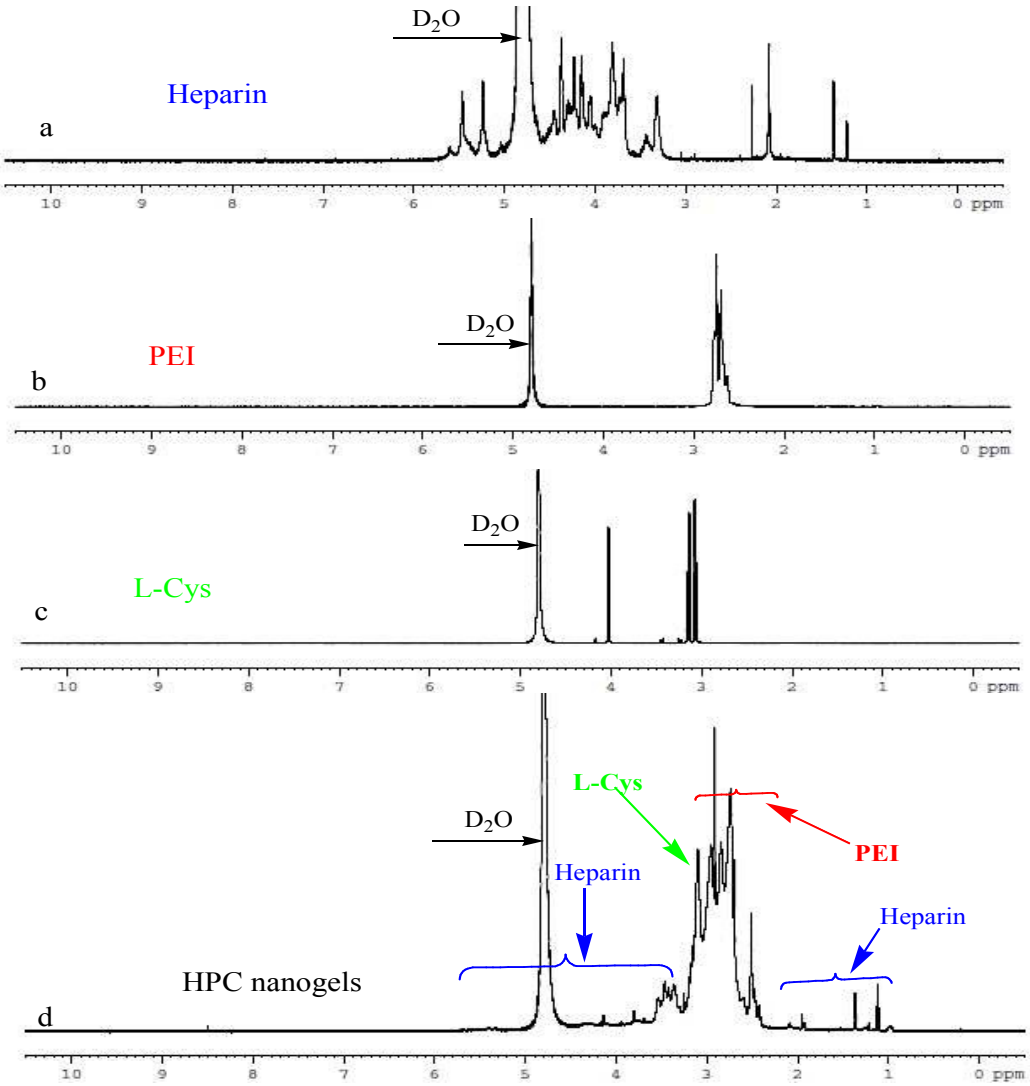


**Figure 2**. $^{1}$H-NMR spectra of a) heparin, b) PEI, c) L-cysteine, and d) $HPC_{0.75}$ nanogel dissolved in the $D_2O$ solvents.

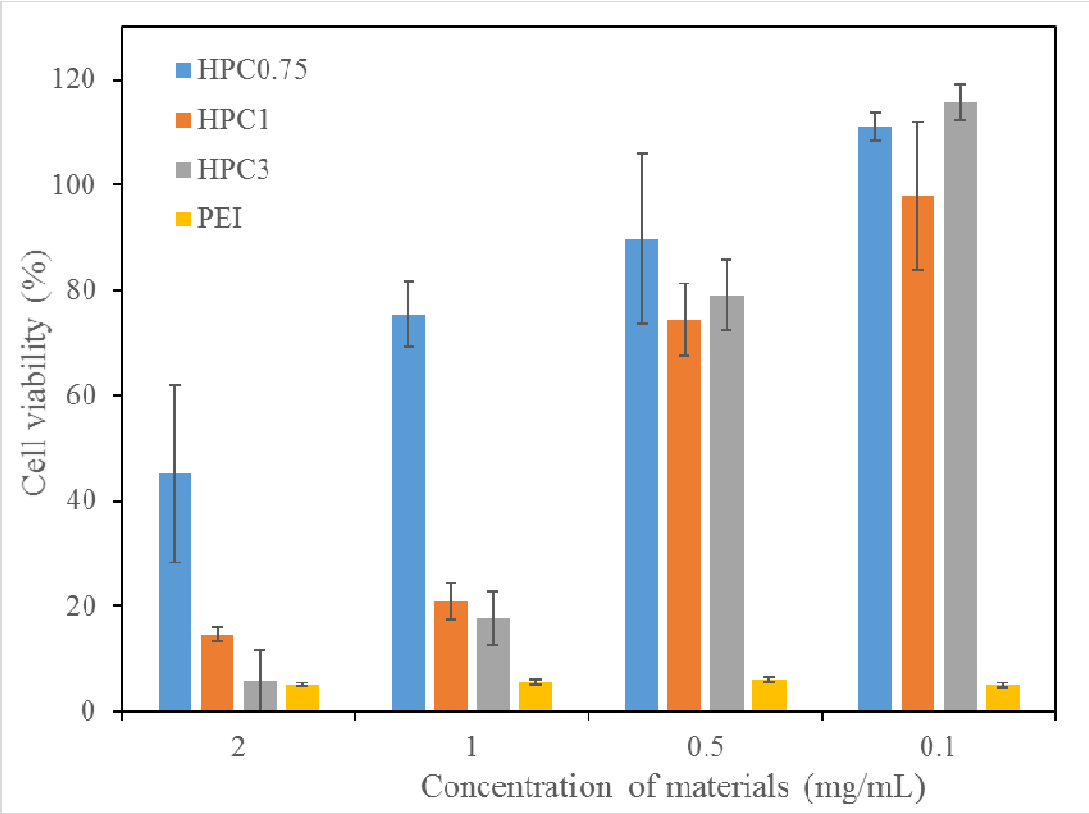


Figure 3. Cell toxicity of various HPC nanogels and branched 25kDa PEI, the data are express as mean ± SD, were n=3

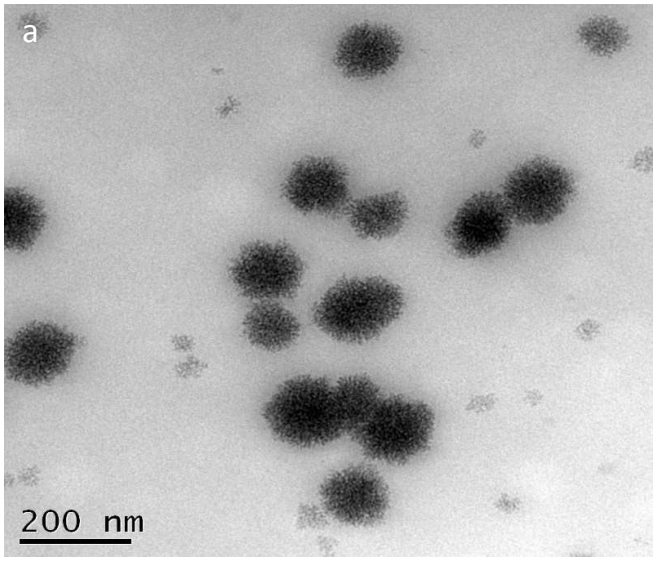


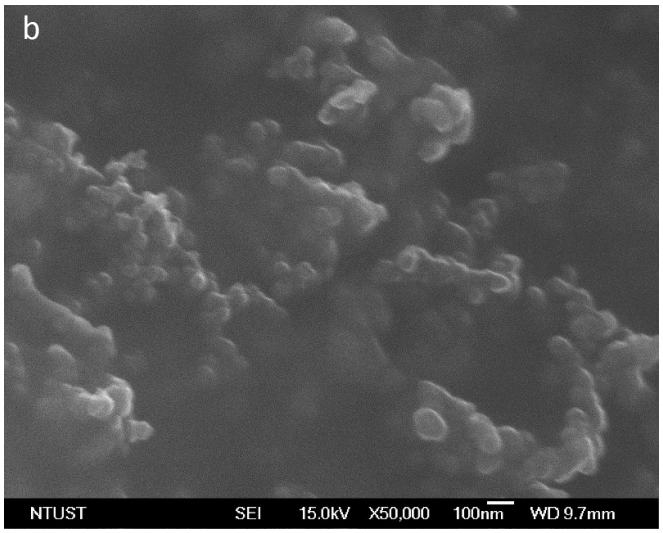


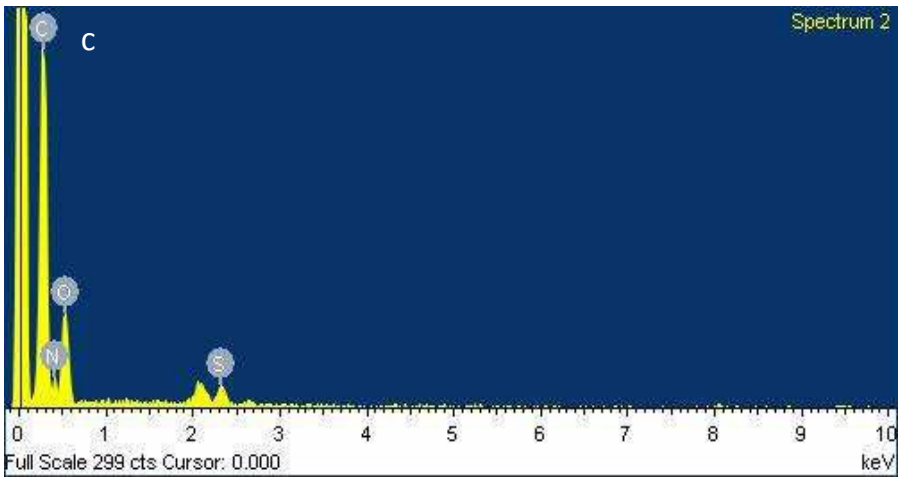


**Figure 4.** Characterization of HPC nanogel: a) TEM, b) FE-SEM, and c) FE-SEM- EDS-elemental composition at selected points

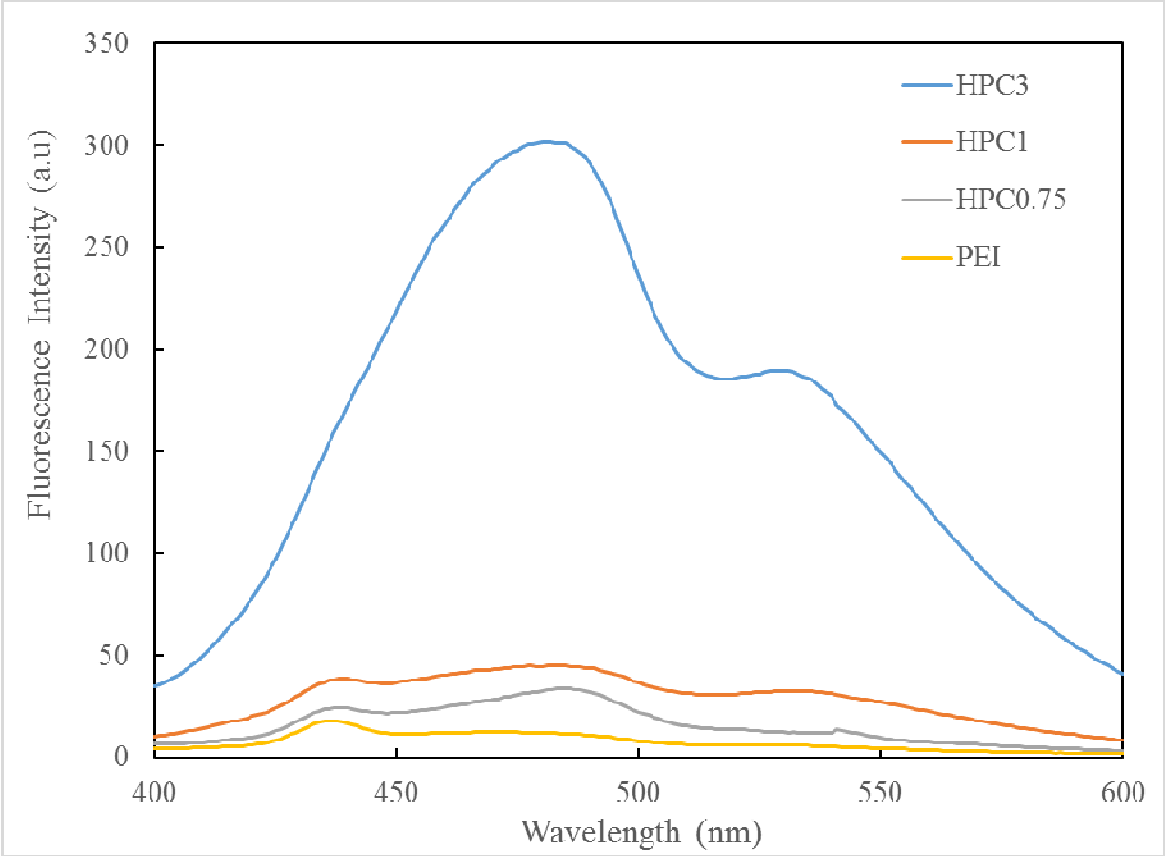


**Figure 5**. Fluorescence intensity of PEI and HPC nanogels at different weight ratios. Note: $HPC_{0.75}$, $HPC_1$, and $HPC_3$ represent nanogels prepared using different composition ratios (w/w) of heparin: PEI: L-Cys (1:0.75:0.75, 1:1:1, 1:3:3) respectively.

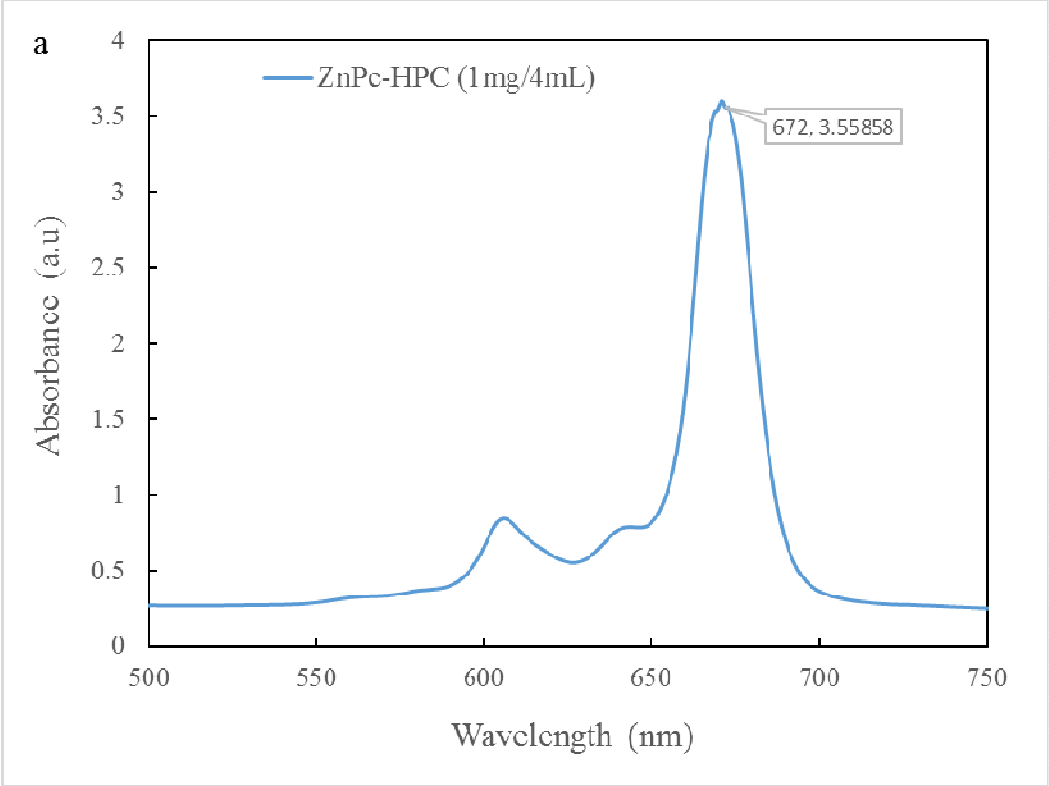


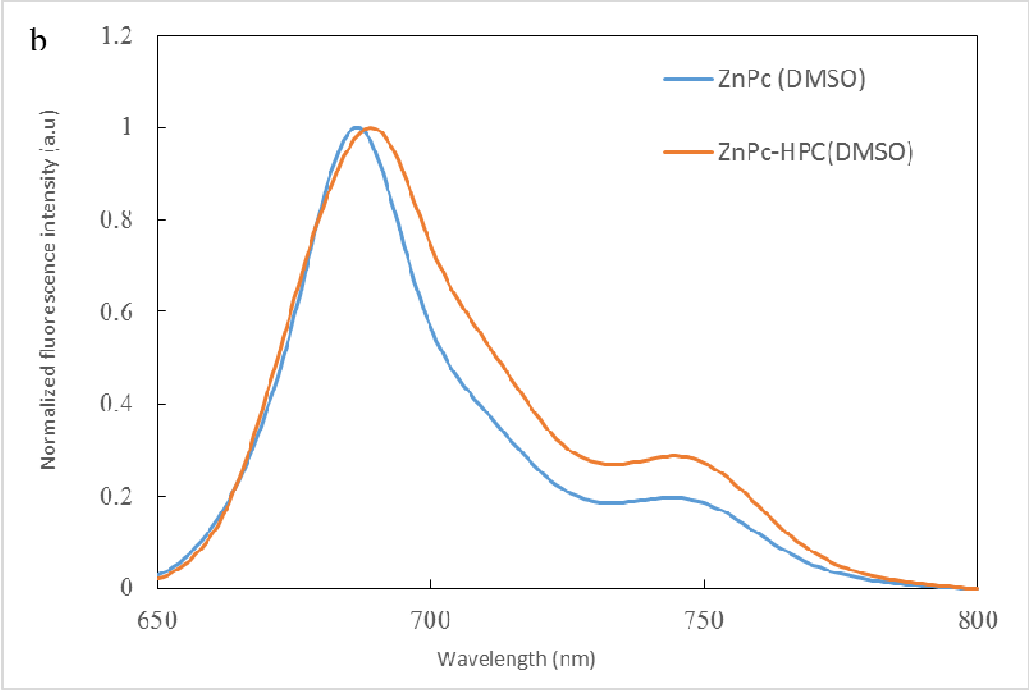


**Figure 6**. a) UV-Vis spectrum of extracted ZnPc from ZnPc-loaded nanogel. b) Fluorescence emission of free ZnPc and ZnPc loaded in HPC nanogels in DMSO

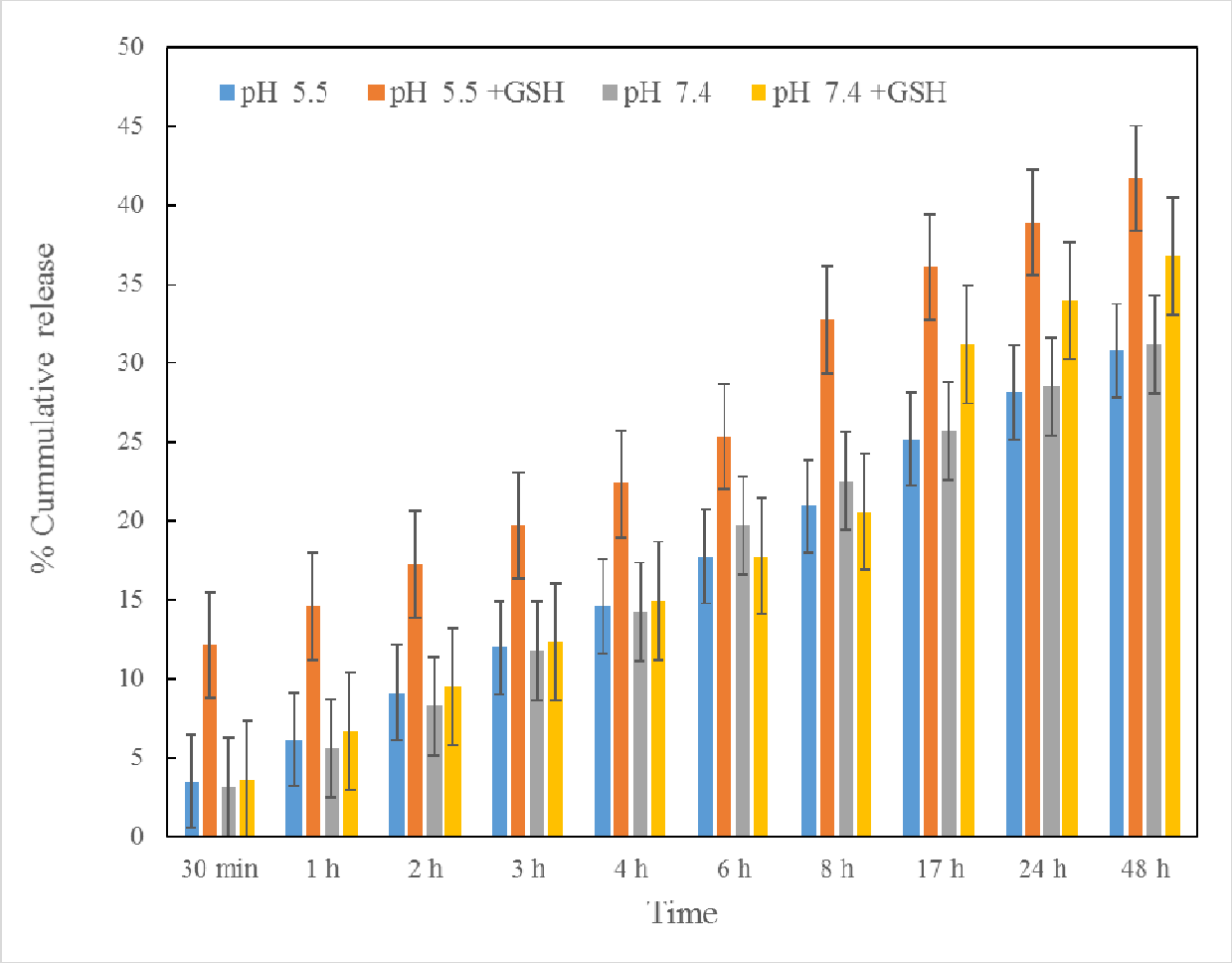


**Figure 7.** In vitro release profiles of ZnPc loaded in HPC nanogels and submerged in 0.01M MES buffers with pH values of 5.5 and 7.4 in the presence and absence of GSH (2mg/mL). The data are express as mean ± SD, were n=3

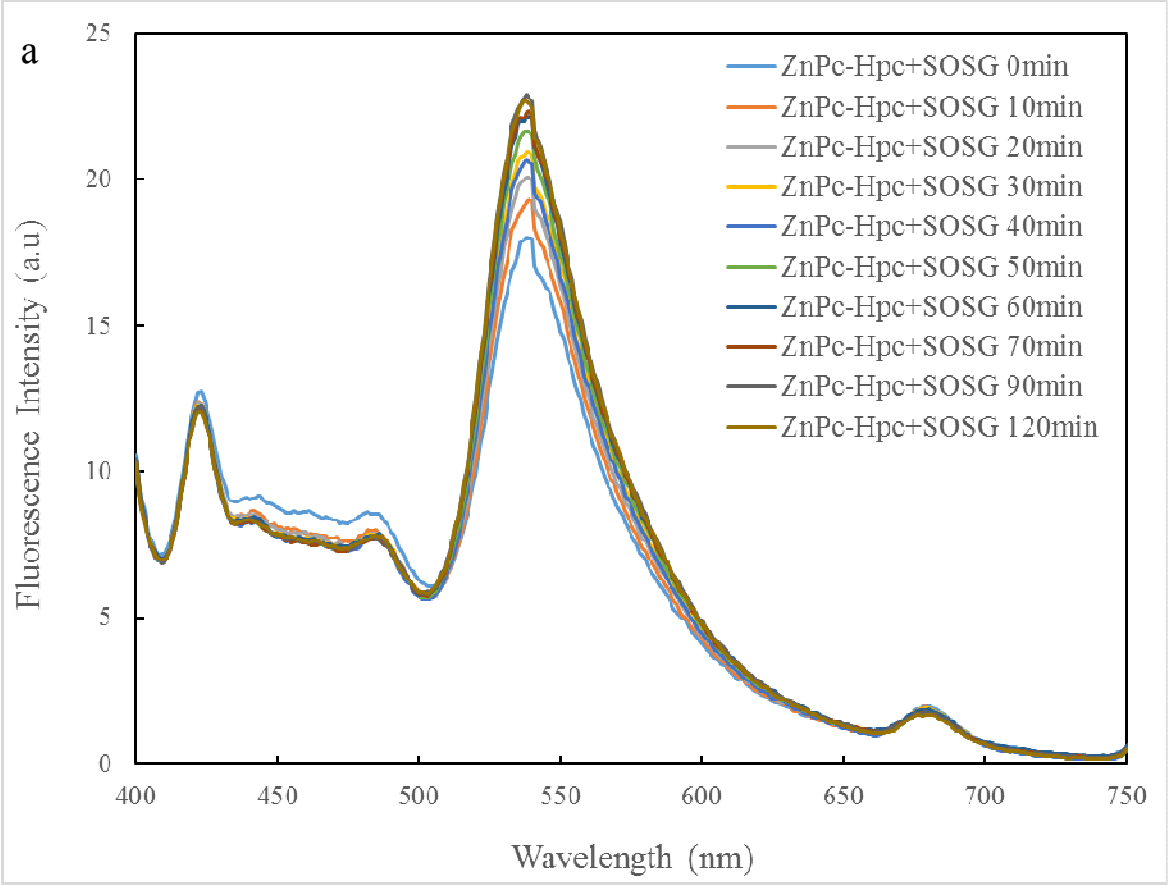


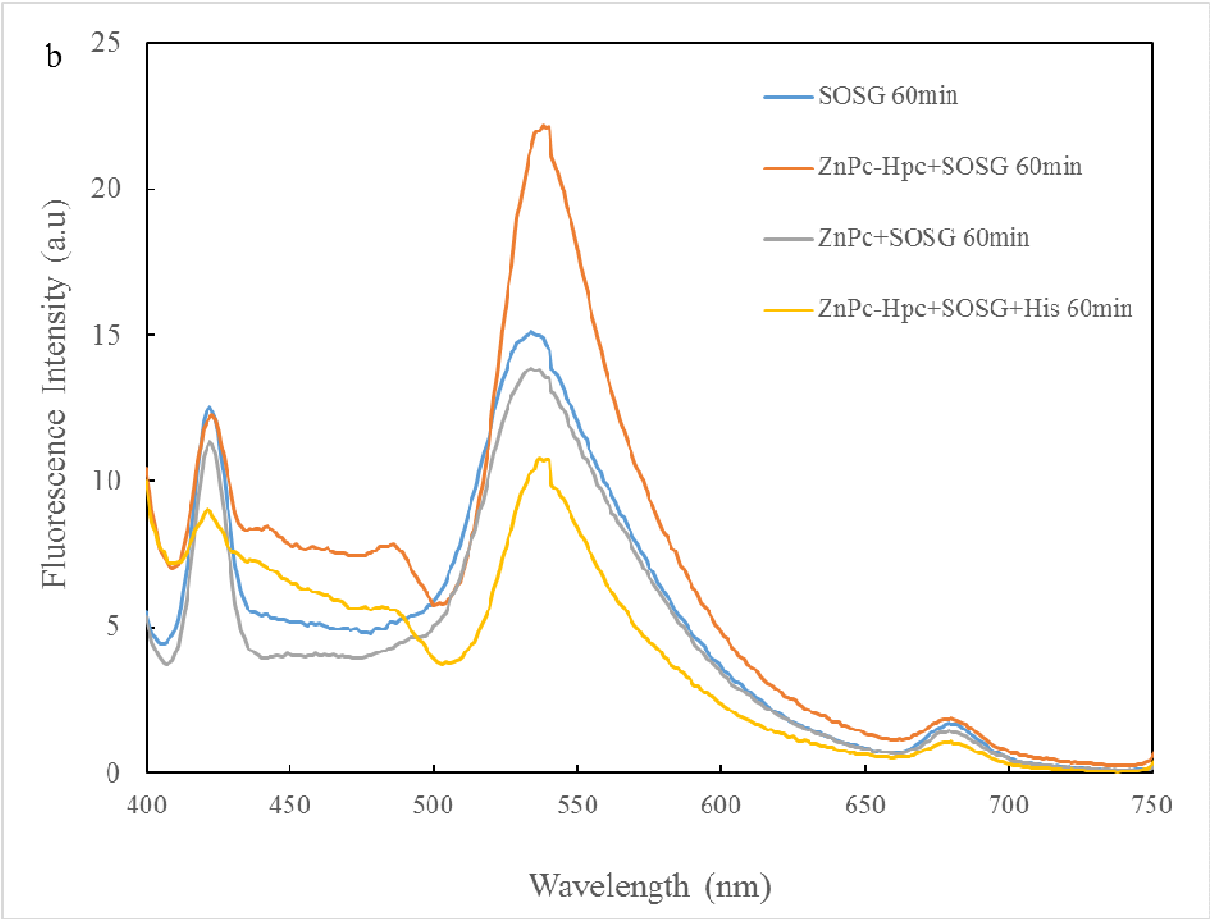

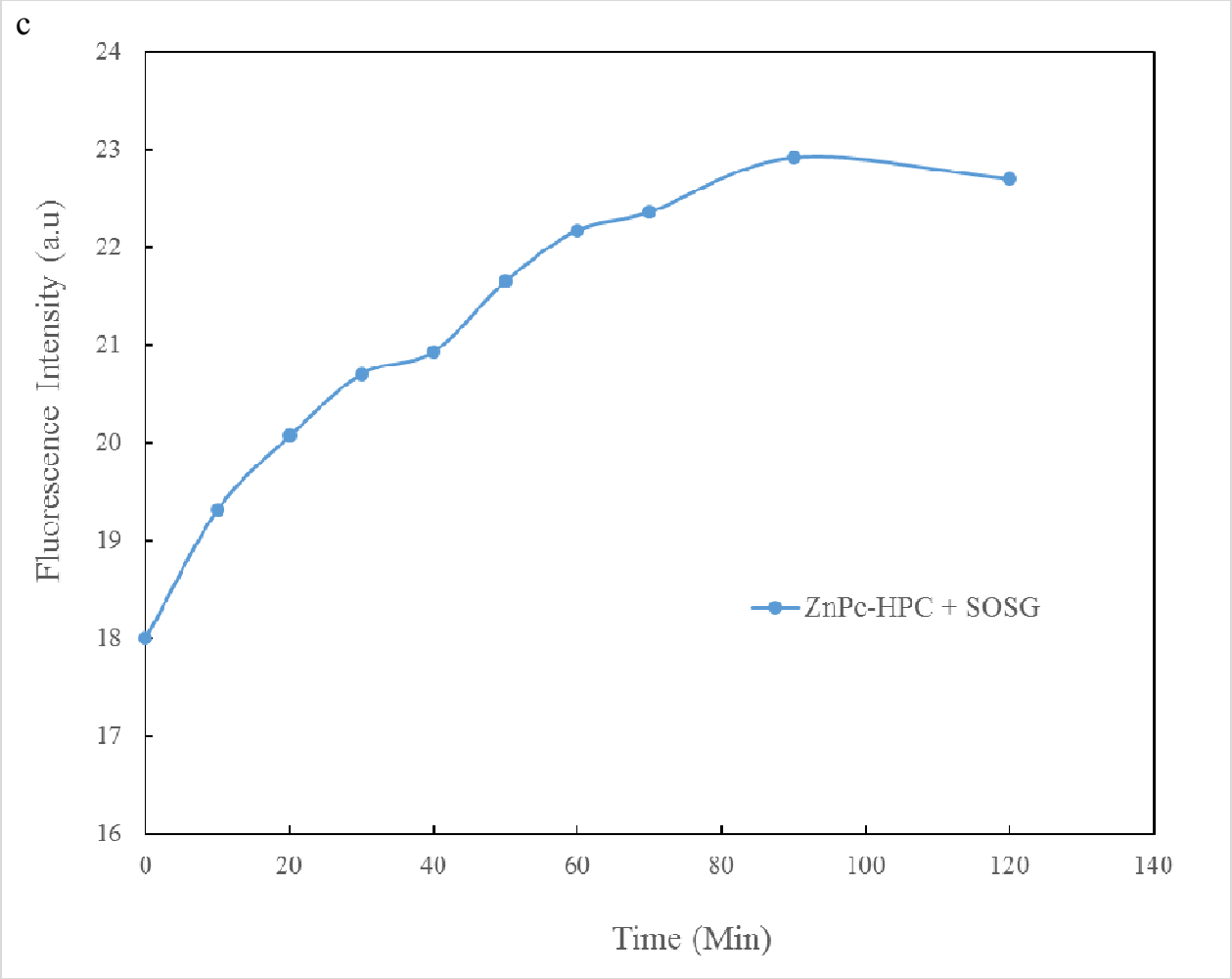


**Figure 8**. Detection of singlet oxygen generation using SOSG. a) Fluorescence emission spectra of SOSG a) before (0 minutes) and after (10-120minutes) reaction with $^1O_2$ generated from 1µM ZnPc loaded in HPC. b) Fluorescence emission spectra of SOSG, ZnPc-HPC-SOSG, ZnPc-SOSG, and ZnPc-HPC-SOSG-His after 60 minutes of irradiation. Increment of fluorescence intensity of ZnPc-HPC-SOSG from 0-120minutes. **Note:** SOSG working reagents (1µM SOSG) was prepared by dissolving 1µL of SOSG from stock solution (5mM) in 5mL of $D_2O$. SOSG fluorescence emission was produced using an excitation wavelength of 482 nm.

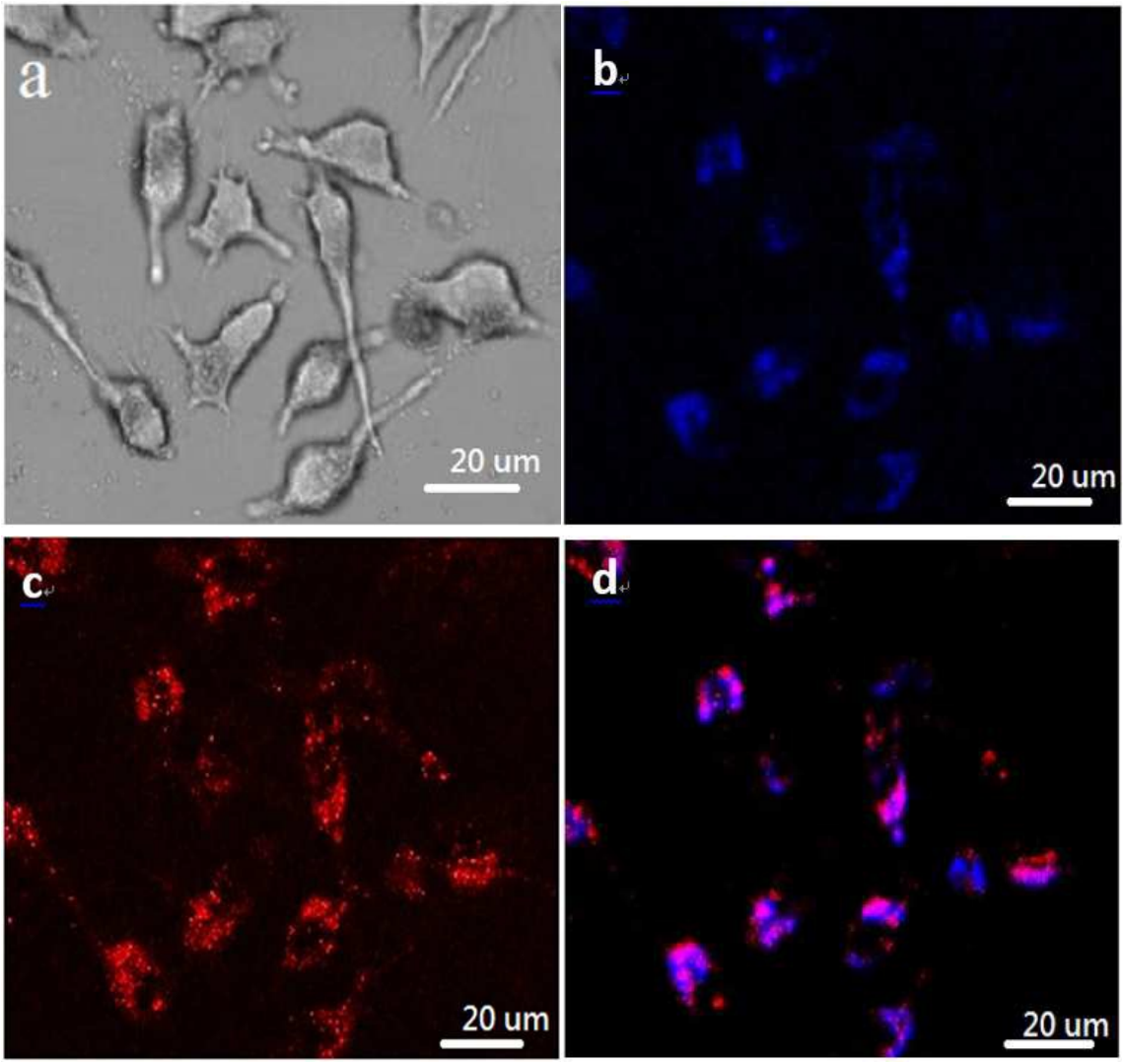


**Figure 9.** Confocal microscopy images of HeLa cells incubated with 0.01mM of ZnPc-HPC nanogels at 37$^{o}$c for 24hrs. a) Bright field image of HeLa cells. b) HPC nanogels up taken by HeLa cells (blue fluorescence: nanogel). c) ZnPc dispersed in the cytosol of HeLa cells (red fluorescence: ZnPc). d) Merged image of ZnPc loaded HPC nanogels. The scale bar is 28.1 μm.

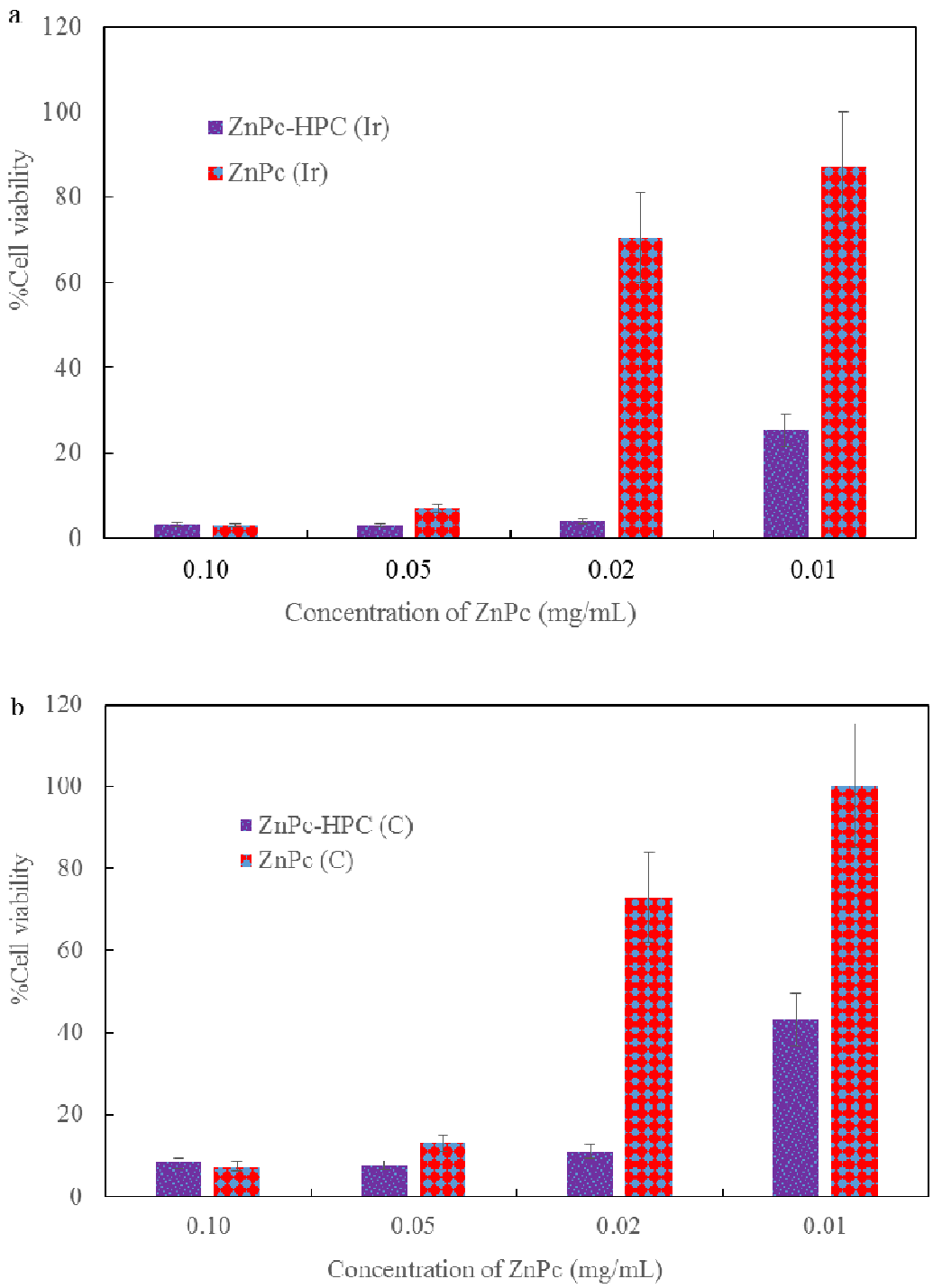


**Figure 10.** Cell viability after PDT. a) Toxicity of ZnPc (Ir) and ZnPc-HPC (Ir) after light irradiation with 532nm laser light for 1hr. b) Toxicity of ZnPc (C) and ZnPc-HPC (C) in dark after 24hr of incubation. Note: ZnPc-HPC (C) and ZnPc (C) represents control in dark area, whereas ZnPc-HPC (Ir) and ZnPc (Ir) represent single light exposure. The data are express as mean ± SD, were n=3

**Table 1.** The mean particle size, PDI and zeta-potential of HPC nanogels prepared with different feeding ratio at 37°C (average particle size and zeta potential is presented as mean ± SD (n = 3))

| S/No | Nanogels Sample | Weight ratio (mg) of **Hep:PEI:Cys** | PDI | Particle size (nm) | Zeta potential (mV) |
|---|---|---|---|---|---|
| 1 | $HPC_{0.75}$ | 1:0.75:0.75 | 0.179 ± 0.119 | 165.7 ± 5.8 | 35.47 ± 1.04 |
| 2 | $HPC_1$ | 1:1:1 | 0.717 ± 0.252 | 134.6 ± 49.9 | 43.4 ± 1.32 |
| 3 | $HPC_3$ | 1:3:3 | 0.55 ± 0.11 | 117.4 ± 20.6 | 48.5 ± 0.4 |
| 4 | ZnPc-$HPC_{0.75}$ | 1:0.75:0.75 | 0.246 ± 0.129 | 97.3 ± 4.94 | 46.33 ± 1.05 |
| 5 | Heparin | 2mg/ml | NA | NA | -61 ± 1.78 |
| 6 | PEI | 2mg/ml | NA | NA | 27.33 ± 0.76 |

**Graphical abstract**